TEMPORALLY DETAILED HYPERGRAPH NEURAL ODES FOR TYPE 2 DIABETES PROGRESSION MODELING

Anonymous authors
Paper under double-blind review

ABSTRACT

Disease progression modeling aims to characterize and predict how a patient's disease complications worsen over time based on longitudinal electronic health records (EHRs). Accurate modeling of disease progression, such as type 2 diabetes, can enhance patient sub-phenotyping and inform effective and timely interventions. However, the problem is challenging due to the need to learn continuous-time dynamics of progression patterns based on irregular-time event samples and patient heterogeneity (*e.g.,* different progression rates and pathways). Existing mechanistic and data-driven methods either lack adaptability to learn from real-world data or fail to capture complex continuous-time dynamics on progression trajectories. To address these limitations, we propose **T**emporally **D**etailed **H**ypergraph **N**eural **O**rdinary **D**ifferential **E**quation (**TD-HNODE**), which represents disease progression on clinically recognized trajectories as a temporally detailed hypergraph and learns the continuous-time progression dynamics via a neural ODE framework. TD-HNODE contains a learnable TD-Hypergraph Laplacian that captures the interdependency of disease complication markers within both intra- and inter-progression trajectories. Experiments on two real-world clinical datasets demonstrate that TD-HNODE outperforms multiple baselines in modeling the progression of type 2 diabetes and related cardiovascular diseases.

1 INTRODUCTION

Many chronic diseases follow a progressive trajectory with multiple complications that worsen over time (Uddin et al., 2023). For example, one patient with type 2 diabetes may gradually develop retinopathy, which advances to visual impairment and eventually to blindness. Another patient may develop hypertension, then atrial fibrillation, and ultimately heart failure. Other patients may experience complications on both trajectories. Disease progression modeling aims to characterize and predict how a patient's disease complications worsen over time based on longitudinal electronic health records (EHRs) (Mould, 2012; Wang et al., 2014). Specifically, given a patient's historical clinical visit records, each associated with a risk factor feature vector (*e.g.,* lab order, medications) and a target complication marker vector (*e.g.,* whether the patient has hypertension, atrial fibrillation, or cerebrovascular disease), the machine learning model needs to predict the complication marker vector for the next visit, so that the progression of these complication markers follows a set of clinically verified trajectories. Disease progression modeling plays a crucial role in patient sub-phenotyping (*i.e.,* grouping patients into categories based on heterogeneous progression patterns) and informing effective and timely treatment (Buil-Bruna et al., 2015; Prague et al., 2013).

However, the problem poses several technical challenges. First, patient records of hospital visits are often sampled at irregular time points, although the underlying disease conditions evolve in continuous time. Second, many chronic and progressive diseases—such as type 2 diabetes, Alzheimer's disease, chronic kidney disease (CKD), cancer (*e.g.,* breast or prostate), and cardiovascular diseases—have clinically recognized progression trajectories that are routinely used to guide prognosis, monitoring, and treatment planning. Building upon these validated pathways is crucial as it aligns with current clinical practice and enhances both the applicability and interoperability of machine learning systems in real-world settings. Third, the progression dynamics are heterogeneous among patients, as reflected by the varying progression rates and progression trajectories (*e.g.,* some patients rapidly develop kidney damage while others remain stable for many years, and some patients may experience neuropathy followed by a foot ulcer).

Existing works on disease progression modeling can be broadly categorized into mechanistic and data-driven approaches (Cook and Bies, 2016; Mould, 2012). Mechanistic models (van Schaick et al., 2015; Shahar, 1995) incorporate biological, pathophysiological, and pharmacological processes into the modeling structure, providing enhanced interpretability but with limited adaptability to real-world data. Data-driven approaches can be further divided into traditional machine learning and deep learning. Traditional machine learning methods often use hidden Markov models (Jackson et al., 2003; Sukkar et al., 2012; Liu et al., 2015) to capture transition probabilities between disease stages, but they often rely on strong assumptions about data distribution at known progression stages and cannot learn implicit stages based on complex feature representations. With increasing electronic health records (EHRs) being collected over the last decade, deep learning methods have been widely developed (Shickel et al., 2017; Solares et al., 2020), including recurrent neural networks (*e.g.,* LSTM) (Zhang, 2019; Zhang et al., 2019; Sohn et al., 2020), attention-based models (*e.g.,* Transformers) (Zisser and Aran, 2024; Zhang, 2019), and Neural Ordinary Differential Equations (Neural ODEs) (Chen et al., 2018; Goyal and Benner, 2023; Chen et al., 2024a). Neural ODE models can capture the continuous-time dynamics of disease progression based on irregular-time clinical events, but existing models (Qian et al., 2021; Dang et al., 2023) fail to incorporate the clinically verified progression pathways. Continuous-time graph neural networks (Rossi et al., 2020; Tian et al., 2021; Liu et al., 2024; Cheng et al., 2024) can potentially represent known progression trajectories as a directed graph, where nodes are complication markers and temporal edges represent progression between them, but a normal graph only captures pairwise interactions (between one complication and its immediate predecessor or successor) and thus miss high-order interactions across all complication nodes along a trajectory (pathway) (Yoon et al., 2020).

To address these limitations, we propose the Temporally Detailed Hypergraph Neural Ordinary Differential Equation (TD-HNODE), which models disease progression along clinically verified trajectories as a temporally detailed hypergraph and learns the continuous-time progression dynamics via a neural ODE framework. Specifically, TD-HNODE consists of two components: (1) a temporally detailed hypergraph (TD-Hypergraph), whereby each node denotes a complication marker and each hyperedge captures temporal dynamics of complication markers (nodes) along a clinically verified progression trajectory (pathway); (2) a Neural ODE module that learns these continuous-time progression dynamics from irregular-time patient records. It is worth noting that our proposed framework differs from existing temporal hypergraph neural networks (Lee and Shin, 2023; Liu et al., 2022; Lee and Shin, 2021), which assign timestamps at the level of entire hyperedges, failing to capture the fine-grained temporal progression details within each hyperedge. Although some methods adopt recurrent modules (*e.g.,* RNNs (Wang et al., 2024a; Younis and Ahmadi, 2024)) and others incorporate continuous-time dynamics (*e.g.,* Neural ODEs (Yao et al., 2023)), they still construct hypergraph snapshots over discrete intervals, where hyperedges remain static units without modeling marker-level timestamps. Detailed experiments on two real-world EHR datasets demonstrate that TD-HNODE outperforms baselines in modeling the progression of type 2 diabetes and related cardiovascular diseases.

2 PROBLEM STATEMENT

2.1 PRELIMINARIES

A patient's medical history can be represented as a sequence of hospital visits called **encounters**. We denote an encounter for patient u at time t_k as $\{\mathbf{x}_u(t_k); \mathbf{y}_u(t_k)\}$, where $\mathbf{x}_u(t_k) \in \mathbb{R}^{c \times 1}$ is a vector of **risk factors**, such as medications, laboratory test results, and vital signs, and $\mathbf{y}_u(t_k) \in \{0,1\}^{n \times 1}$ is a vector of **disease complication markers** (1 for presence, 0 for absence), such as hypertension (HP), atrial fibrillation (AF), heart failure (HF), cerebrovascular disease (CD), and stroke (S). The set of all n markers is denoted as $\mathcal{V} = \{v_i \mid i = 1, \ldots, n\}$.

The marker vector $\mathbf{y}_u(t)$ evolves over time in the encounter sequence of patient u, reflecting the progression of disease states. How the markers evolve follows a set of **disease progression trajectories** (or **pathways**) that can be constructed based on clinical knowledge. Formally, a trajectory is defined as an ordered sequence of distinct markers, denoted as $p_j =< v_1^j, v_2^j, ..., v_{|p_j|}^j >$, where

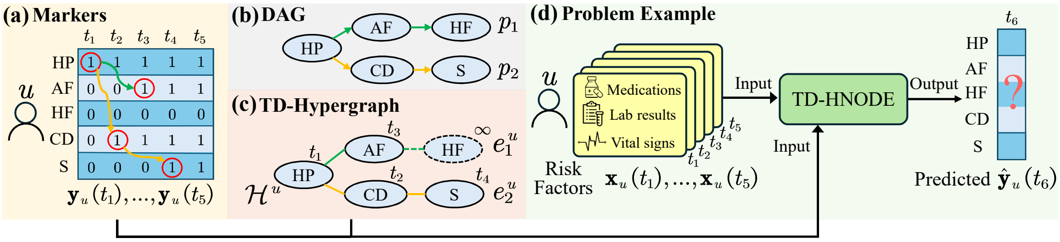

	t_1	t_2	t_3	t_4	t_5
HP	1	1	1	1	1
AF	0	0	1	1	1
HF	0	0	0	0	0
CD	0	1	1	1	1
S	0	0	0	1	1

Figure 1: (a) Patient u's marker status vector from t_1 to t_5; (b) The corresponding DAG of trajectories p_1 and p_2; (c) Patient u's TD-Hypergraph with two temporally detailed hyperedges e_1^u, e_2^u; (d) An example of problem definition showing TD-HNODE's input and output.

$v_i^j \in \mathcal{V}$ represents the i-th marker in the j-th trajectory, and $|p_j|$ is the number of markers. We assume that the disease markers in the trajectory are **irreversible**, *i.e.,* the binary status of markers can only transit from 0 to 1 (or stay the same) within an encounter sequence. This assumption is reasonable, as many chronic diseases—such as Alzheimer's disease, Parkinson's disease, chronic kidney disease (CKD), type 2 diabetes, and chronic obstructive pulmonary disease (COPD)—exhibit irreversible progression (*e.g.,* neuronal loss, organ fibrosis, vascular damage); thus, it is essential to model patient-specific and temporally evolving disease trajectories to support early and personalized interventions (Wu et al., 2021; Kazemian et al., 2019; Bhatwadekar et al., 2021; Wang et al., 2024b).

Figure 1(a) provides an example of the temporal records of a patient's five disease complication markers (HP, AF, HF, CD, and S) from t_1 to t_5. Figure 1(b) shows two clinically known progression trajectories (in green and yellow) that these markers follow, *i.e.,* $p_1 =< HP, AF, HF >$ and $p_2 =< HP, CD, S >$. The fact that the patient's markers follow these trajectories is highlighted by the red circles as well as the green and yellow arrows in Figure 1(a). For instance, once the patient has hypertension ($HP = 1$) at time t_1, the status will persist. The patient's disease progresses from hypertension to cerebrovascular disease ($CD = 1$) at time t_2 and to stroke ($S = 1$) at t_4, following the yellow trajectory. Similarly, the disease progresses from hypertension to atrial fibrillation at t_3 ($AF = 1$) following the green trajectory. Note that the patient's disease complication markers have not yet progressed to heart failure (HF) by t_5, but it could happen at a future time.

The set of clinically known progression trajectories forms a Directed Acyclic Graph (DAG), as illustrated in Figure 1(b). To capture the higher-order marker patterns within trajectories, we propose to represent trajectories using a hypergraph (Gallo et al., 1993). Specifically, we represent the set of markers within the same trajectory as a hyperedge. There are two key advantages: (1) a hyperedge can connect multiple markers in an entire trajectory (pathway), enabling the modeling of high-order dependencies beyond pairwise relations (Feng et al., 2019; Gao et al., 2022); and (2) different hyperedges overlap with each other through common markers (potentially pivotal nodes) (Chitra and Raphael, 2019), making it easier to model interdependency across progression pathways.

We formally define the **disease progression hypergraph** as $\mathcal{H} = (\mathcal{V}, \mathcal{E})$, where $\mathcal{V}$ is the set of **markers**, also referred to as **nodes** throughout the paper, and $\mathcal{E}$ denotes the set of hyperedges, each corresponding to a predefined trajectory (we use the terms 'hyperedge', 'pathway', and 'trajectory' interchangeably). Specifically, $\mathcal{E} = \{e_1, e_2, \ldots, e_m\}$, and $e_j = \{v_1^j, v_2^j, \ldots, v_{|e_j|}^j\}$, where m is the total number of predefined trajectories, and $|e_j|$ is the number of markers in the j-th trajectory.

We define a **temporally detailed trajectory** as the actual progression of markers of a patient u over time. Formally, $p_j^u =< (v_1^j, t_1), (v_2^j, t_2), \cdots, (v_{|p_j^u|}^j, t_{|p_j^u|}) >$, where p_j^u represents patient u's realized progression along trajectory p_j, v_i^j is the i-th marker in the trajectory p_j, t_i is the timestamp when marker v_i^j first appeared in the patient's encounter sequence, and $|p_j^u|$ is the number of markers observed in the j-th trajectory for patient u. Since a patient may not develop all markers in a predefined trajectory, the length $|p_j^u|$ of a temporally detailed trajectory can be shorter than the full trajectory length $|p_j|$. For example, as shown in Figure 1(a), the two temporally detailed trajectories identified for patient u up to timestamp t_5 are $p_1^u =< (HP, t_1), (AF, t_3) >$ (shorter than the full potential trajectory $p_1 =< HP, AF, HF >$) and $p_2^u =< (HP, t_1), (CD, t_2), (S, t_4) >$.

A **Temporally Detailed Hypergraph (TD-Hypergraph)** is formally defined as $\mathcal{H}^u = (\mathcal{V}, \mathcal{E}^u)$, where $\mathcal{V}$ is the set of nodes, and $\mathcal{E}^u$ is the set of temporally detailed hyperedges, with each hyperedge corresponding to a patient-specific temporally detailed trajectory. Specifically, $\mathcal{E}^u = \{e_1^u, e_2^u, \ldots, e_m^u\}$, and $e_j^u = \{(v_1^j, t_1), (v_2^j, t_2), \ldots, (v_k^j, t_k), (v_{k+1}^j, \infty), \ldots, (v_{|e_j|}^j, \infty)\}$, where m is the total number of predefined trajectories, and each hyperedge e_j^u encodes markers with their corresponding timestamps. We assume that up to the latest observed timestamp t_k, the patient u's j-th trajectory has progressed to marker v_k^j. The placeholder ∞ indicates that the remaining markers in a hyperedge have not been observed yet. Figure 1(c) provides an example of the TD-Hypergraph at time t_5 corresponding to the patient u in Figure 1(a)–(b). By the time t_5, the markers have progressed to S (stroke) but not HF (heart failure) yet. The TD-Hypergraph of a patient is time-dependent. It evolves with the progression of complication markers over time, as represented by the updates of timestamps (temporal details) on hyperedges (trajectories).

A list of commonly used notations is provided in Table 3 (Appendix A).

2.2 PROBLEM DEFINITION

Given patient encounter data with risk factors $\{\mathbf{x}_u(t_1), \ldots, \mathbf{x}_u(t_k)\}_{u=1}^N$ and target complication markers $\{\mathbf{y}_u(t_1), \ldots, \mathbf{y}_u(t_k); \mathbf{y}_u(t_{k+1})\}_{u=1}^N$, and the TD-Hypergraph $\{\mathcal{H}^u\}_{u=1}^N$, the problem aims to learn a TD-HNODE model f_θ such that $\hat{\mathbf{y}}_u(t_{k+1}) = f_\theta\left(\mathbf{x}_u(t_1), \ldots, \mathbf{x}_u(t_k), \mathbf{y}_u(t_1), \ldots, \mathbf{y}_u(t_k);\ \mathcal{H}^u\right)$. The objective is to minimize the loss $\min_\theta \frac{1}{N}\sum_{u=1}^N \mathcal{L}\left(\hat{\mathbf{y}}_u(t_{k+1}), \mathbf{y}_u(t_{k+1})\right)$. Figure 1(d) provides an illustrative example. The TD-HNODE model takes as input patient u's risk factors $\mathbf{x}_u(t_1), \ldots, \mathbf{x}_u(t_5)$ (*e.g.,* medications, lab results, and vital signs, Figure 1(d) left), marker status $\mathbf{y}_u(t_1), \ldots, \mathbf{y}_u(t_5)$ (Figure 1(a)), and a TD-Hypergraph $\mathcal{H}^u$ (Figure 1(c)). The model predicts future marker status at t_6 (Figure 1(d) right).

3 METHODOLOGY

An overview of our model framework: To incorporate prior clinical knowledge of disease progression trajectories, we designed TD-HNODE, where nodes represent complication markers and hyperedges represent patient progression trajectories across the markers. As shown in Figure 2(a), TD-HNODE employs Neural ODE to capture continuous progression from irregular-time encounters (patient index u omitted for simplicity). At each time step t_k, risk factors $\mathbf{x}(t_k)$ and complication markers $\mathbf{y}(t_k)$ are embedded into node representations of the temporally detailed hypergraph $\mathcal{H}^u$. The embedded features and progression timestamps were used to construct a learnable TD-Hypergraph Laplacian (Figure 2(b)), capturing intra-trajectory dynamics and inter-trajectory dependencies. Let $\mathbf{S}(t) \in \mathbb{R}^{n\times d}$ denote the hidden state of markers at time t, where n is the number of markers and d is the embedding dimension. The learnable TD-Hypergraph Laplacian $\tilde{\mathbf{L}}(t)$, together with current risk factors $\mathbf{x}(t_k)$ and hidden state representation $\mathbf{S}(t_k)$, was passed to the Neural ODE solver to update the latent state $\mathbf{S}(t_{k+1})$ for the next time step t_{k+1}, which was then decoded to predict disease complication marker status $\hat{\mathbf{y}}(t_{k+1})$.

3.1 NEURAL ODE AND HYPERGRAPH NEURAL NETWORK

We started with an introduction to a Neural ODE, which learns a continuous dynamic function $\mathbf{S}(t)$:

$$\frac{d\,\mathbf{S}(t)}{dt} = f\big(t, \mathbf{S}(t), \mathbf{x}(t); \mathbf{\Theta}\big), \tag{1}$$

where $\mathbf{\Theta}$ are learnable parameters, and $f(\cdot)$ is a neural network that models the temporal gradient of the disease state. We initialized the hidden state $\mathbf{S}(t_1)$ based on the patient's initial marker status and risk factors at time t_1.

To infuse clinical domain knowledge of disease progression pathways into the Neural ODE framework and capture high-order dependencies among disease markers, we proposed to integrate a hypergraph Laplacian $\mathbf{L}$ inspired by Hypergraph Neural Networks (Feng et al., 2019). It enabled multi-way message passing over disease trajectories. The resulting ODE dynamics were defined as follows:

$$\frac{d\,\mathbf{S}(t)}{dt} = -\,\mathbf{L}\left[\mathbf{S}(t) + h\big(\mathbf{x}(t)\big)\right]\mathbf{\Theta}, \tag{2}$$

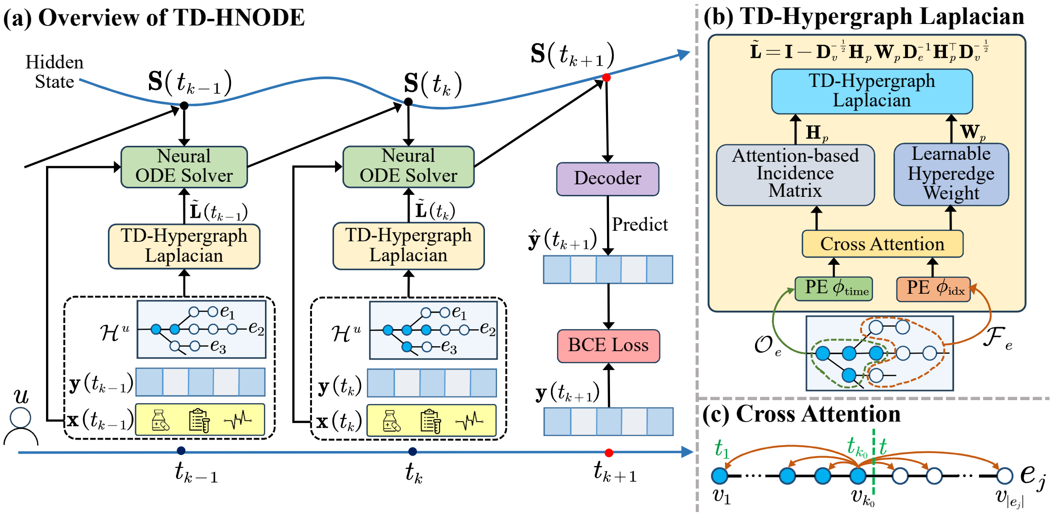

Figure 2: (a) Overview of the TD-HNODE, with an example of patient u's encounter sequence; (b) The TD-Hypergraph Laplacian module combining an Attention-based Incidence Matrix and a Learnable Hyperedge Weight Matrix; (c) An illustration of cross attention within hyperedge e_j.

where $h(\cdot)$ maps $\mathbf{x}(t)$ into the same space as $\mathbf{S}(t)$, and $\mathbf{\Theta} \in \mathbb{R}^{d\times d}$ is a learnable transformation matrix. The negative sign simulates diffusion-like propagation among markers (Ji et al., 2022). The common hypergraph Laplacian $\mathbf{L}$ is defined as:

$$\mathbf{L} = \mathbf{I} - \mathbf{D}_v^{-1/2}\mathbf{H}\mathbf{W}\mathbf{D}_e^{-1}\mathbf{H}^\top\mathbf{D}_v^{-1/2}, \tag{3}$$

where $\mathbf{H} \in \{0,1\}^{n\times m}$ is the incidence matrix with $\mathbf{H}(i,e) = 1$ if marker v_i belongs to hyperedge e, and $\mathbf{H}(i,e) = 0$ otherwise. $\mathbf{W} \in \mathbb{R}^{m\times m}$ is a diagonal hyperedge weight matrix. The node and hyperedge degree matrices are $\mathbf{D}_v(i,i) = \sum_e \mathbf{H}(i,e)\,\mathbf{W}(e,e)$, and $\mathbf{D}_e(e,e) = \sum_i \mathbf{H}(i,e)$.

However, the initial formulation above uses a static incidence matrix $\mathbf{H}$ and treats all nodes equally within each hyperedge. In addition, it relies on fixed diagonal hyperedge weight matrices $\mathbf{W} \in \mathbb{R}^{m\times m}$. These simplifications fail to capture several important characteristics of disease progression modeling: (1) the relative importance of markers within a trajectory may evolve over time; and (2) inter-trajectory dependencies due to shared markers and correlated temporal dynamics. In the following section, we extend this formulation into a learnable TD-Hypergraph Laplacian, which is temporally adaptive and tailored to patient-specific progression patterns.

3.2 LEARNABLE TD-HYPERGRAPH LAPLACIAN

We proposed two key enhancements: (1) Attention-based Incidence Matrix: we replaced the binary incidence matrix with a learnable attention mechanism, allowing the model to assign time-aware, patient-specific importance to each marker node within a progression trajectory; (2) Learnable Hyperedge Weights: instead of assigning fixed weights to hyperedges, we introduced learnable weights that captured inter-trajectory dependencies based on shared markers and correlation patterns. This design allowed TD-HNODE to perform high-order message passing guided by clinical knowledge while adapting to patient-specific disease trajectories.

3.2.1 ATTENTION-BASED INCIDENCE MATRIX

To account for temporal dynamics and the varying importance of markers in a trajectory, we designed an adaptive incidence matrix based on cross-attention within each temporally detailed hyperedge. Given a temporally detailed hyperedge $e_j = \{(v_1^j, t_1), (v_2^j, t_2), \ldots, (v_{k_0}^j, t_{k_0}), (v_{k_0+1}^j, \infty), \ldots, (v_{|e_j|}^j, \infty)\}$, we denoted the current progression point at time t_{k_0} as v_{k_0}, omitting the trajectory index j for notational simplicity. Based on this, we split e_j into two subsets: a *past set* $\mathcal{O}_e^j = \{v_1, ..., v_{k_0}\}$, and a *potential set* $\mathcal{F}_e^j = \{v_{k_0+1}, ..., v_{|e_j|}\}$ (since we had not yet observed the actual occurrence of the complication markers yet).

Each marker $v_i \in e_j$ had an initial embedding $\mathbf{b}_i \in \mathbb{R}^d$, which captured its identity information within the trajectory. Specifically, $\mathbf{b}_i$ was obtained by applying a learnable multilayer perceptron to the one-hot encoding of the marker v_i. To incorporate temporal order, we applied different positional encodings depending on whether the marker had been observed: $\phi(i) = \phi_{\text{time}}(t_i)$ if $v_i \in \mathcal{O}_e^j$, and $\phi(i) = \phi_{\text{idx}}(i)$ if $v_i \in \mathcal{F}_e^j$, where $\phi_{\text{time}}(t_i) \in \mathbb{R}^d$ was a continuous-time encoding (Xu et al., 2020), and $\phi_{\text{idx}}(i) \in \mathbb{R}^d$ was a discrete index-based encoding (Vaswani et al., 2017).

We computed the query vectors as:

$$\mathbf{q}_i^{\text{time}} = (\mathbf{b}_i + \phi_{\text{time}}(t_i))\mathbf{W}_Q \quad \text{if } v_i \in \mathcal{O}_e^j, \tag{4}$$

$$\mathbf{q}_i^{\text{idx}} = (\mathbf{b}_i + \phi_{\text{idx}}(i))\mathbf{W}_Q \quad \text{if } v_i \in \mathcal{F}_e^j, \tag{5}$$

where $\mathbf{W}_Q \in \mathbb{R}^{d\times d}$ is a learnable projection matrix. Key and value vectors $\mathbf{k}_i^{\text{time}}, \mathbf{k}_i^{\text{idx}}, \mathbf{v}_i^{\text{time}}, \mathbf{v}_i^{\text{idx}} \in \mathbb{R}^d$ for all markers $v_i \in e_j$ were constructed in the same way, using the respective positional encodings and projection matrices $\mathbf{W}_K, \mathbf{W}_V \in \mathbb{R}^{d\times d}$.

We then computed the attention weights from v_{k_0} to all other markers $v_i \in e_j$ using:

$$\alpha_e(i, k_0) = \begin{cases} \dfrac{\exp(\mathbf{q}_{k_0}^{\text{time}} \cdot \mathbf{k}_i^{\text{time}}/\sqrt{d})}{\sum\limits_{l\in\mathcal{O}_e} \exp(\mathbf{q}_{k_0}^{\text{time}} \cdot \mathbf{k}_l^{\text{time}}/\sqrt{d})} & \text{if } i \le k_0, \\ \dfrac{\exp(\mathbf{q}_{k_0}^{\text{idx}} \cdot \mathbf{k}_i^{\text{idx}}/\sqrt{d})}{\sum\limits_{l\in\mathcal{F}_e} \exp(\mathbf{q}_{k_0}^{\text{idx}} \cdot \mathbf{k}_l^{\text{idx}}/\sqrt{d})} & \text{if } i > k_0. \end{cases} \tag{6}$$

This attention mechanism allowed the model to differentiate between observed and unobserved markers, assigning context-aware, time-sensitive weights within each hyperedge. We then constructed the adaptive incidence matrix $\mathbf{H}_p$ by modulating each entry with the cross-attention weight from the current marker v_{k_0} to the marker v_i:

$$\mathbf{H}_p(i, e) = \begin{cases} \mathbf{H}(i, e) \cdot \alpha_e(i, k_0) & \text{if } v_i \in e, \\ 0 & \text{otherwise.} \end{cases} \tag{7}$$

Here, $\alpha_e(i, k_0)$ encodes the directional and time-aware importance of marker v_i under the current progression context. This formulation allows the incidence matrix to capture both structural relations and temporal dynamics, reflecting the evolving role of each marker during disease progression.

3.2.2 LEARNABLE HYPEREDGE WEIGHT MATRIX

Traditional hypergraph-based methods typically assume a fixed hyperedge weight matrix $\mathbf{W} \in \mathbb{R}^{m\times m}$, where m is the number of hyperedges. However, this assumption fails to capture variable correlation strengths in patient-specific progression across trajectories. To address this, we introduced a learnable hyperedge weight matrix $\mathbf{W}_p \in \mathbb{R}^{m\times m}$ based on hyperedge representation, which modeled dynamic dependencies among trajectories. The key idea was to derive trajectory-level embeddings from their constituent markers and compute trajectory similarity in a learned latent space.

For each marker $v_i \in e_j$, we computed its context-enhanced representation $\tilde{\mathbf{v}}_i$ using self-attention within the subset it belongs to. Specifically, self-attention was performed separately over the past set $\mathcal{O}_e^j$ and the future set $\mathcal{F}_e^j$, producing $\tilde{\mathbf{v}}_i = \text{SelfAttn}(v_i, \mathcal{O}_e^j)$ if $v_i \in \mathcal{O}_e^j$, and $\tilde{\mathbf{v}}_i = \text{SelfAttn}(v_i, \mathcal{F}_e^j)$ if $v_i \in \mathcal{F}_e^j$. Here, $\text{SelfAttn}(v_i, \cdot)$ denotes standard scaled dot-product attention with v_i as query and all other markers in the same subset as keys and values. The resulting vector $\tilde{\mathbf{v}}_i \in \mathbb{R}^d$ captured context-specific information and was used to form hyperedge-level representations. Specifically, for hyperedge $e_j \in \mathcal{E}$, we aggregated the value vectors $\tilde{\mathbf{v}}_i$ to obtain a trajectory-level representation:

$$\mathbf{g}_j = \text{Aggregate}\big\{\tilde{\mathbf{v}}_i \mid v_i \in e_j\big\}, \tag{8}$$

where $\text{Aggregate}(\cdot)$ is a differentiable pooling function, such as average pooling.

We aggregated the trajectory-level embeddings from all hyperedges $\mathcal{E}$ into trajectory embedding matrix $\mathbf{G} = [...; \mathbf{g}_j; ...] \in \mathbb{R}^{m\times d}$, where the j-th row of $\mathbf{G}$, *i.e.,* , $\mathbf{g}_j$, encoded the representation of the j-th trajectory (hyperedge). We then projected this matrix into a latent space using a trainable linear transformation: $\tilde{\mathbf{G}} = \mathbf{G}\mathbf{W}_{\mathcal{E}}$, where $\mathbf{W}_{\mathcal{E}} \in \mathbb{R}^{d \times d}$. The latent trajectory embedding matrix $\tilde{\mathbf{G}}$ was then used to compute the trajectory correlation matrix, also called *learnable hyperedge weight matrix*:

$$\mathbf{W}_p = \tilde{\mathbf{G}}\tilde{\mathbf{G}}^T \in \mathbb{R}^{m \times m}. \tag{9}$$

This learnable matrix $\mathbf{W}_p$ captures data-driven similarities between all trajectories, allowing the model to emphasize more relevant progression pathways as well as their interdependency.

We combined the adaptive incidence $\mathbf{H}_p$ and the learnable hyperedge weight matrix $\mathbf{W}_p$ to form our Knowledge-Infused TD-Hypergraph Laplacian:

$$\tilde{\mathbf{L}} = \mathbf{I} - \mathbf{D}_v^{-\frac{1}{2}} \mathbf{H}_p \mathbf{W}_p \mathbf{D}_e^{-1} \mathbf{H}_p^{\top} \mathbf{D}_v^{-\frac{1}{2}}, \tag{10}$$

where $\mathbf{I}$ is the $n \times n$ identity matrix. In this way, $\tilde{\mathbf{L}}$ encodes intra-trajectory time-sensitive marker dependencies (through $\mathbf{H}_p$) and inter-trajectory correlations (through $\mathbf{W}_p$). Note that $\tilde{\mathbf{L}}$, $\mathbf{H}_p$, and $\mathbf{W}_p$ all depend on the current time t, since the current progression marker timestamp t_{k_0} on each hyperedge is determined by the time point t. To reflect continuous-time progression, we rewrote $\tilde{\mathbf{L}}$ into a time-dependent form $\tilde{\mathbf{L}}(t)$, which was recomputed at each integration step t to reflect the evolving patient state and hypergraph structure. Substituting $\tilde{\mathbf{L}}(t)$ into Eq. (2) yields our final knowledge-infused disease progression model:

$$\frac{d\,\mathbf{S}(t)}{dt} = -\,\tilde{\mathbf{L}}(t)\,\big[\mathbf{S}(t) + h\big(\mathbf{x}(t)\big)\big]\,\boldsymbol{\Theta}. \tag{11}$$

The complete training procedure and pseudocode are provided in Appendix B, while the **computational complexity analysis** is detailed in Appendix C.

4 EXPERIMENTS

4.1 EXPERIMENTAL SETUP

Datasets. We conducted experiments on two EHR datasets: (1) a clinical dataset collected from a regional medical network affiliated with our institution, referred to as the *University Hospital* dataset; and (2) *MIMIC-IV* (Johnson et al., 2023), a publicly accessible EHR dataset. We extracted 34 risk factors associated with the progression of diabetes and its complications, as detailed in Table 4 (Appendix D.1), and identified 21 outcome markers of diabetes complications $\mathcal{V}$, as summarized in Table 5 (Appendix D.2). We also constructed a disease progression hypergraph $\mathcal{H}$ based on expert-validated clinical pathways provided by our clinical collaborators, as detailed in Appendix D.3. The *University Hospital* and *MIMIC-IV* datasets contained 2,415 patients and 902 patient sequences, respectively. More details are provided in Appendix D.4.

Baselines. To evaluate TD-HNODE, we compared it with representative baselines across four categories. For **Sequential Models**, we included T-LSTM (Baytas et al., 2017), which handles irregular visits using time-aware LSTM, and ContiFormer (Chen et al., 2024b), which redefines self-attention over evolving latent trajectories. For **Temporal Graph Neural Networks**, we used discrete-time MegaCRN (Jiang et al., 2023) and continuous-time TGNE (Cheng et al., 2024), which model temporal graphs via snapshots and event-based messages, respectively. For **Temporal Hypergraph Neural Networks**, we compared with DHSL (Wang et al., 2024a), which fuses hypergraph convolution with GRU, and HyperTime (Younis and Ahmadi, 2024), which builds dynamic hypergraphs with LSTM-enhanced hyperedge convolutions. For **Neural ODE-based Models**, we included NODE (Chen et al., 2018), capturing continuous dynamics in latent space, and CODE-RNN (Coelho et al., 2025), which integrates ODEs with RNNs for time-series modeling. Full baselines implementation details are provided in Appendix D.6.

We evaluated performance using Accuracy, Precision, Recall, and F1-score, emphasizing Recall due to class imbalance and the need to detect early progression. High Recall reflects better identification of true positives, critical for clinical deployment. Source code has been included in the Supplementary Material for reproducibility, and implementation detailes are provided in Appendix D.5.

Table 1: Results (%, average ± std) of all methods on *University Hospital* dataset and *MIMIC-IV* dataset, with the best results in bold.

Methods	University Hospital				MIMIC-IV			
	Accuracy	Precision	Recall	F1-score	Accuracy	Precision	Recall	F1-score
T-LSTM	69.2$_{\pm 0.4}$	10.6$_{\pm 0.2}$	55.7$_{\pm 0.2}$	12.8$_{\pm 0.1}$	84.1$_{\pm 0.2}$	17.0$_{\pm 0.5}$	58.2$_{\pm 0.1}$	24.5$_{\pm 0.3}$
ContiFormer	77.2$_{\pm 0.2}$	12.3$_{\pm 0.1}$	65.4$_{\pm 0.2}$	16.7$_{\pm 0.2}$	86.2$_{\pm 0.1}$	26.2$_{\pm 0.4}$	82.1$_{\pm 0.2}$	36.5$_{\pm 0.3}$
MegaCRN	70.7$_{\pm 0.1}$	8.1$_{\pm 0.1}$	64.5$_{\pm 0.6}$	12.9$_{\pm 0.1}$	83.4$_{\pm 0.5}$	22.4$_{\pm 0.3}$	70.1$_{\pm 1.3}$	30.8$_{\pm 0.4}$
TGNE	72.4$_{\pm 0.2}$	8.6$_{\pm 0.1}$	75.4$_{\pm 0.3}$	14.2$_{\pm 0.1}$	85.0$_{\pm 0.5}$	23.4$_{\pm 0.1}$	72.8$_{\pm 0.2}$	32.1$_{\pm 0.2}$
DHSL	72.8$_{\pm 0.1}$	8.3$_{\pm 0.1}$	60.5$_{\pm 0.3}$	13.5$_{\pm 0.3}$	82.9$_{\pm 0.2}$	22.0$_{\pm 0.2}$	69.9$_{\pm 0.3}$	29.8$_{\pm 0.2}$
HyperTime	74.9$_{\pm 0.2}$	9.3$_{\pm 0.1}$	59.0$_{\pm 0.1}$	13.9$_{\pm 0.1}$	84.6$_{\pm 0.2}$	25.1$_{\pm 0.1}$	71.4$_{\pm 0.2}$	31.7$_{\pm 0.2}$
NODE	72.3$_{\pm 0.1}$	10.7$_{\pm 0.3}$	56.9$_{\pm 0.1}$	14.4$_{\pm 0.3}$	84.4$_{\pm 0.2}$	19.5$_{\pm 0.3}$	62.3$_{\pm 0.2}$	27.2$_{\pm 0.1}$
CODE-RNN	73.0$_{\pm 0.1}$	10.0$_{\pm 0.1}$	61.5$_{\pm 0.2}$	15.0$_{\pm 0.1}$	85.7$_{\pm 0.1}$	23.5$_{\pm 0.2}$	74.5$_{\pm 0.4}$	32.5$_{\pm 0.2}$
TD-HNODE	**79.4**$_{\pm 0.1}$	**14.3**$_{\pm 0.2}$	**79.3**$_{\pm 0.3}$	**20.4**$_{\pm 0.4}$	**87.9**$_{\pm 0.1}$	**31.8**$_{\pm 0.4}$	**85.7**$_{\pm 0.4}$	**42.9**$_{\pm 1.3}$

Table 2: Ablation study results (%) of TD-HNODE on *University Hospital* and *MIMIC-IV* dataset.

$\mathbf{H}_p$	$\mathbf{W}_p$	University Hospital				MIMIC-IV			
		Accuracy	Precision	Recall	F1-score	Accuracy	Precision	Recall	F1-score
✓	✓	79.4	14.3	79.3	20.4	87.9	31.8	85.7	42.9
✗	✓	75.3	12.9	77.0	18.9	86.1	27.7	78.5	36.6
✓	✗	76.5	11.5	79.2	18.7	86.8	29.0	84.9	38.5
✗	✗	73.1	10.6	76.1	15.5	83.0	23.3	73.1	30.8

4.2 COMPARISON ON CLASSIFICATION PERFORMANCE

We compared TD-HNODE with all baselines on the *University Hospital* and *MIMIC-IV* datasets, with results summarized in Table 1. TD-HNODE consistently achieved the best performance across all metrics. On *University Hospital*, it outperformed the strongest baseline (ContiFormer) by 2.2% in accuracy and 3.7% in F1-score, and by 1.7% and 6.4% on *MIMIC-IV*. Compared to non-structural models like T-LSTM, NODE, and CODE-RNN, TD-HNODE showed substantial Recall and F1 gains (*e.g.,* +23.4% Recall over NODE on *MIMIC-IV*), demonstrating its strength in capturing complex disease dynamics through its trajectory-aware hypergraph structure. TD-HNODE also surpassed temporal structure models such as MegaCRN and TGNE. Notably, it achieved 3.9% and 12.9% Recall improvements over TGNE on *University Hospital* and *MIMIC-IV*, respectively. These results confirmed that modeling high-order multi-node interactions via hyperedges offered stronger representational power than traditional pairwise edges, enabling more accurate and clinically meaningful early disease prediction with fewer false negatives.

Additional experiments on cardiovascular disease are provided in Appendix D.7, further demonstrating the generalizability of TD-HNODE beyond diabetes.

4.3 ABLATION STUDY

We assessed the impact of two core components in TD-HNODE: the **adaptive incidence matrix** $\mathbf{H}_p$ and the **learnable hyperedge weights** $\mathbf{W}_p$. As shown in Table 2, using $\mathbf{H}_p$ improved F1-score from 15.5% to 18.7% without $\mathbf{W}_p$, and to 20.4% with it, highlighting the benefit of intra-trajectory attention for time-aware marker importance. Meanwhile, enabling $\mathbf{W}_p$ boosted recall from 76.1% to 77.0% and F1-score from 15.5% to 18.9% even with static $\mathbf{H}$, and yielded 5.4%/5.8% gains on recall/F1 on *MIMIC-IV*, validating the value of modeling inter-trajectory dependencies.

4.4 SENSITIVITY ANALYSIS

We analyzed TD-HNODE's sensitivity to two hyperparameters: embedding dimension d and the number of ODE solver steps in RK4. As shown in Figure 3(a), increasing d from 64 to 128 significantly improved recall (*e.g.,* from 0.747 to 0.857 on *MIMIC-IV*), but further increases showed diminishing returns or overfitting, so we chose $d = 128$. Similarly, Figure 3(b) shows that varying the number of steps from 4 to 12 revealed underfitting at lower values (*e.g.,* 4 or 6), while

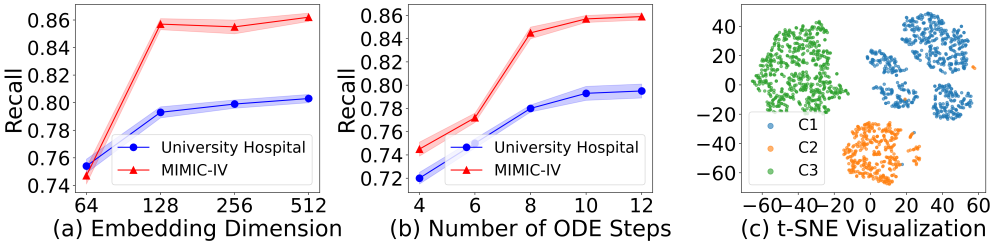

(a) Embedding Dimension (b) Number of ODE Steps (c) t-SNE Visualization

Figure 3: (a) Recall of TD-HNODE on both datasets with varying embedding dimensions. (b) Recall with varying numbers of ODE steps. (c) t-SNE visualization of 1,690 patients from the *University Hospital* dataset; C1, C2, and C3 denote Clusters 1, 2, and 3.

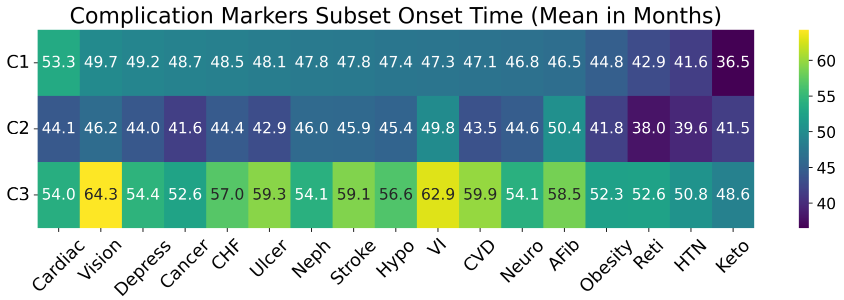
Complication Markers Subset Onset Time (Mean in Months)

	Cardiac	Vision	Depress	Cancer	CHF	Ulcer	Neph	Stroke	Hypo	VI	CVD	Neuro	AFib	Obesity	Reti	HTN	Keto
C1	53.3	49.7	49.2	48.7	48.5	48.1	47.8	47.8	47.4	47.3	47.1	46.8	46.5	44.8	42.9	41.6	36.5
C2	44.1	46.2	44.0	41.6	44.4	42.9	46.0	45.9	45.4	49.8	43.5	44.6	50.4	41.8	38.0	39.6	41.5
C3	54.0	64.3	54.4	52.6	57.0	59.3	54.1	59.1	56.6	62.9	59.9	54.1	58.5	52.3	52.6	50.8	48.6

Figure 4: Mean onset time (in months from the first encounter) of each marker across patients in each cluster. Earlier values indicate earlier manifestation or faster progression.

performance stabilized around 10 steps with minimal gains beyond. These results confirmed TD-HNODE's robustness and the suitability of its default hyperparameter settings for real-world EHR applications.

4.5 CASE STUDY

We conducted a case study to apply the TD-HNODE results for patient progression sub-phenotyping. Specifically, we extracted the patient embeddings (prior to the decoder layers) learned from TD-HNODE on the *University Hospital* dataset. We visualized the patient embeddings in 2D using t-SNE projection and identified three clear clusters, as shown in Figure 3(c). We then used hierarchical clustering to group patients into these three clusters and analyzed disease progression patterns within each cluster. Specifically, for each of the 21 complication markers, we computed the *mean onset time* (in months since the first encounter) for patients within each cluster. A smaller onset time indicated faster progression of complication outcomes. As shown in Figure 4, patients in Cluster 3 exhibited the slowest progression, followed by Cluster 1, and then Cluster 2, which showed the most rapid progression. For example, compared to Cluster 3, patients in Cluster 2 experienced earlier onset by 9 months in *Cardiac Revascularization (Cardiac)*, 18 months in *Blindness and Vision Loss (Vision)*, and 12 months in *Congestive Heart Failure (CHF)*. These results demonstrated that TD-HNODE effectively captures the heterogeneity within the patient cohort.

5 CONCLUSION AND FUTURE WORK

In this work, we proposed TD-HNODE, a novel framework for continuous-time disease progression modeling that integrates medical knowledge with a TD-hypergraph-based Neural ODE. The method captures both intra- and inter-trajectory dependencies, and experiments on real-world EHR datasets demonstrated its effectiveness in modeling diabetes progression. For future work, our framework currently focuses on known disease progression pathways, as in chronic diseases such as diabetes, and should be extended to infer unknown or partially characterized trajectories (*e.g.,* via frequent pattern mining or Bayesian networks). In addition, we plan to incorporate causal inference to evaluate the impact of complex treatment regimens.

REFERENCES

Shahadat Uddin, Shangzhou Wang, Arif Khan, and Haohui Lu. Comorbidity progression patterns of major chronic diseases: the impact of age, gender and time-window. *Chronic Illness*, 19(2): 304–313, 2023.

DR Mould. Models for disease progression: new approaches and uses. *Clinical Pharmacology & Therapeutics*, 92(1):125–131, 2012.

Xiang Wang, David Sontag, and Fei Wang. Unsupervised learning of disease progression models. In *Proceedings of the 20th ACM SIGKDD international conference on Knowledge discovery and data mining*, pages 85–94, 2014.

Núria Buil-Bruna, Tarjinder Sahota, José-María López-Picazo, Marta Moreno-Jiménez, Salvador Martín-Algarra, Benjamin Ribba, and Iñaki F Trocóniz. Early prediction of disease progression in small cell lung cancer: Toward model-based personalized medicine in oncology. *Cancer research*, 75(12):2416–2425, 2015.

Mélanie Prague, Daniel Commenges, and Rodolphe Thiébaut. Dynamical models of biomarkers and clinical progression for personalized medicine: The hiv context. *Advanced drug delivery reviews*, 65(7):954–965, 2013.

Sarah F Cook and Robert R Bies. Disease progression modeling: key concepts and recent developments. *Current pharmacology reports*, 2:221–230, 2016.

Erno van Schaick, Jenny Zheng, Juan Jose Perez Ruixo, Ronald Gieschke, and Philippe Jacqmin. A semi-mechanistic model of bone mineral density and bone turnover based on a circular model of bone remodeling. *Journal of pharmacokinetics and pharmacodynamics*, 42:315–332, 2015.

Yuval Shahar. *A knowledge-based method for temporal abstraction of clinical data*. Stanford University, 1995.

Christopher H Jackson, Linda D Sharples, Simon G Thompson, Stephen W Duffy, and Elisabeth Couto. Multistate markov models for disease progression with classification error. *Journal of the Royal Statistical Society Series D: The Statistician*, 52(2):193–209, 2003.

Rafid Sukkar, Elyse Katz, Yanwei Zhang, David Raunig, and Bradley T Wyman. Disease progression modeling using hidden markov models. In *2012 annual international conference of the IEEE engineering in medicine and biology society*, pages 2845–2848. IEEE, 2012.

Yu-Ying Liu, Shuang Li, Fuxin Li, Le Song, and James M Rehg. Efficient learning of continuous-time hidden markov models for disease progression. *Advances in neural information processing systems*, 28, 2015.

Benjamin Shickel, Patrick James Tighe, Azra Bihorac, and Parisa Rashidi. Deep ehr: a survey of recent advances in deep learning techniques for electronic health record (ehr) analysis. *IEEE journal of biomedical and health informatics*, 22(5):1589–1604, 2017.

Jose Roberto Ayala Solares, Francesca Elisa Diletta Raimondi, Yajie Zhu, Fatemeh Rahimian, Dexter Canoy, Jenny Tran, Ana Catarina Pinho Gomes, Amir H Payberah, Mariagrazia Zottoli, Milad Nazarzadeh, et al. Deep learning for electronic health records: A comparative review of multiple deep neural architectures. *Journal of biomedical informatics*, 101:103337, 2020.

Yuan Zhang. Attain: Attention-based time-aware lstm networks for disease progression modeling. In *In Proceedings of the 28th International Joint Conference on Artificial Intelligence (IJCAI-2019), pp. 4369-4375, Macao, China.*, 2019.

Yuan Zhang, Xi Yang, Julie Ivy, and Min Chi. Time-aware adversarial networks for adapting disease progression modeling. In *2019 IEEE International Conference on Healthcare Informatics (ICHI)*, pages 1–11. IEEE, 2019.

Hyunwoo Sohn, Kyungjin Park, and Min Chi. Mulan: Multilevel language-based representation learning for disease progression modeling. In *2020 IEEE International Conference on Big Data (Big Data)*, pages 1246–1255. IEEE, 2020.

Moshe Zisser and Dvir Aran. Transformer-based time-to-event prediction for chronic kidney disease deterioration. *Journal of the American Medical Informatics Association*, 31(4):980–990, 2024.

Ricky TQ Chen, Yulia Rubanova, Jesse Bettencourt, and David K Duvenaud. Neural ordinary differential equations. *Advances in neural information processing systems*, 31, 2018.

Pawan Goyal and Peter Benner. Neural ordinary differential equations with irregular and noisy data. *Royal Society Open Science*, 10(7):221475, 2023.

Yang Chen, Hong Liu, Pinhao Song, and Wenhao Li. Neural ordinary differential equation for irregular human motion prediction. *Pattern Recognition Letters*, 178:76–83, 2024a.

Zhaozhi Qian, William Zame, Lucas Fleuren, Paul Elbers, and Mihaela van der Schaar. Integrating expert odes into neural odes: pharmacology and disease progression. *Advances in Neural Information Processing Systems*, 34:11364–11383, 2021.

Ting Dang, Jing Han, Tong Xia, Erika Bondareva, Chloë Siegele-Brown, Jagmohan Chauhan, Andreas Grammenos, Dimitris Spathis, Pietro Cicuta, and Cecilia Mascolo. Conditional neural ode processes for individual disease progression forecasting: a case study on covid-19. In *Proceedings of the 29th ACM SIGKDD Conference On Knowledge Discovery and Data Mining*, pages 3914–3925, 2023.

Emanuele Rossi, Ben Chamberlain, Fabrizio Frasca, Davide Eynard, Federico Monti, and Michael Bronstein. Temporal graph networks for deep learning on dynamic graphs. *arXiv preprint arXiv:2006.10637*, 2020.

Sheng Tian, Tao Xiong, and Leilei Shi. Streaming dynamic graph neural networks for continuous-time temporal graph modeling. In *2021 IEEE International Conference on Data Mining (ICDM)*, pages 1361–1366. IEEE, 2021.

Jie Liu, Jiamou Liu, Kaiqi Zhao, Yanni Tang, and Wu Chen. Tp-gnn: Continuous dynamic graph neural network for graph classification. In *2024 IEEE 40th International Conference on Data Engineering (ICDE)*, pages 2848–2861. IEEE, 2024.

Ke Cheng, Junchen Ye, Xiaodong Lu, Leilei Sun, and Bowen Du. Temporal graph network for continuous-time dynamic event sequence. *Knowledge-Based Systems*, 304:112452, 2024.

Se-eun Yoon, Hyungseok Song, Kijung Shin, and Yung Yi. How much and when do we need higher-order information in hypergraphs? a case study on hyperedge prediction. In *Proceedings of the web conference 2020*, pages 2627–2633, 2020.

Geon Lee and Kijung Shin. Temporal hypergraph motifs. *Knowledge and Information Systems*, 65 (4):1549–1586, 2023.

Yunyu Liu, Jianzhu Ma, and Pan Li. Neural predicting higher-order patterns in temporal networks. In *Proceedings of the ACM Web Conference 2022*, pages 1340–1351, 2022.

Geon Lee and Kijung Shin. Thyme+: Temporal hypergraph motifs and fast algorithms for exact counting. In *2021 IEEE international conference on data mining (ICDM)*, pages 310–319. IEEE, 2021.

Shun Wang, Yong Zhang, Xuanqi Lin, Yongli Hu, Qingming Huang, and Baocai Yin. Dynamic hypergraph structure learning for multivariate time series forecasting. *IEEE Transactions on Big Data*, 10(4):556–567, 2024a.

Raneen Younis and Zahra Ahmadi. Hypertime: A dynamic hypergraph approach for time series classification. In *2024 IEEE International Conference on Data Mining (ICDM)*, pages 570–579. IEEE, 2024.

Chengzhi Yao, Zhi Li, and Junbo Wang. Spatio-temporal hypergraph neural ode network for traffic forecasting. In *2023 IEEE International Conference on Data Mining (ICDM)*, pages 1499–1504. IEEE, 2023.

Botong Wu, Sijie Ren, Jing Li, Xinwei Sun, Shi-Ming Li, and Yizhou Wang. Forecasting irreversible disease via progression learning. In *Proceedings of the IEEE/CVF Conference on Computer Vision and Pattern Recognition*, pages 8117–8125, 2021.

Pooyan Kazemian, Jonathan E Helm, Mariel S Lavieri, Joshua D Stein, and Mark P Van Oyen. Dynamic monitoring and control of irreversible chronic diseases with application to glaucoma. *Production and operations management*, 28(5):1082–1107, 2019.

Ashay D Bhatwadekar, Aumer Shughoury, Ameya Belamkar, and Thomas A Ciulla. Genetics of diabetic retinopathy, a leading cause of irreversible blindness in the industrialized world. *Genes*, 12(8):1200, 2021.

Yipei Wang, Bing He, Shannon Risacher, Andrew Saykin, Jingwen Yan, and Xiaoqian Wang. Learning the irreversible progression trajectory of alzheimer's disease. In *2024 IEEE International Symposium on Biomedical Imaging (ISBI)*, pages 1–5. IEEE, 2024b.

Giorgio Gallo, Giustino Longo, Stefano Pallottino, and Sang Nguyen. Directed hypergraphs and applications. *Discrete applied mathematics*, 42(2-3):177–201, 1993.

Yifan Feng, Haoxuan You, Zizhao Zhang, Rongrong Ji, and Yue Gao. Hypergraph neural networks. In *Proceedings of the AAAI conference on artificial intelligence*, volume 33, pages 3558–3565, 2019.

Yue Gao, Yifan Feng, Shuyi Ji, and Rongrong Ji. Hgnn+: General hypergraph neural networks. *IEEE Transactions on Pattern Analysis and Machine Intelligence*, 45(3):3181–3199, 2022.

Uthsav Chitra and Benjamin Raphael. Random walks on hypergraphs with edge-dependent vertex weights. In *International conference on machine learning*, pages 1172–1181. PMLR, 2019.

Jiahao Ji, Jingyuan Wang, Zhe Jiang, Jiawei Jiang, and Hu Zhang. Stden: Towards physics-guided neural networks for traffic flow prediction. In *Proceedings of the AAAI conference on artificial intelligence*, volume 36, pages 4048–4056, 2022.

Da Xu, chuanwei ruan, evren korpeoglu, sushant kumar, and kannan achan. Inductive representation learning on temporal graphs. In *International Conference on Learning Representations (ICLR)*, 2020.

Ashish Vaswani, Noam Shazeer, Niki Parmar, Jakob Uszkoreit, Llion Jones, Aidan N Gomez, Łukasz Kaiser, and Illia Polosukhin. Attention is all you need. *Advances in neural information processing systems*, 30, 2017.

Alistair EW Johnson, Lucas Bulgarelli, Lu Shen, Alvin Gayles, Ayad Shammout, Steven Horng, Tom J Pollard, Sicheng Hao, Benjamin Moody, Brian Gow, et al. Mimic-iv, a freely accessible electronic health record dataset. *Scientific data*, 10(1):1, 2023.

Inci M Baytas, Cao Xiao, Xi Zhang, Fei Wang, Anil K Jain, and Jiayu Zhou. Patient subtyping via time-aware lstm networks. In *Proceedings of the 23rd ACM SIGKDD international conference on knowledge discovery and data mining*, pages 65–74, 2017.

Yuqi Chen, Kan Ren, Yansen Wang, Yuchen Fang, Weiwei Sun, and Dongsheng Li. Contiformer: Continuous-time transformer for irregular time series modeling. *Advances in Neural Information Processing Systems*, 36, 2024b.

Renhe Jiang, Zhaonan Wang, Jiawei Yong, Puneet Jeph, Quanjun Chen, Yasumasa Kobayashi, Xuan Song, Shintaro Fukushima, and Toyotaro Suzumura. Spatio-temporal meta-graph learning for traffic forecasting. In *Proceedings of the AAAI conference on artificial intelligence*, volume 37, pages 8078–8086, 2023.

C Coelho, M Fernanda P Costa, and LL Ferrás. Neural chronos ode: Modeling bidirectional temporal patterns in time-series data. *Expert Systems with Applications*, page 126784, 2025.

Dunya Tomic, Jonathan E Shaw, and Dianna J Magliano. The burden and risks of emerging complications of diabetes mellitus. *Nature Reviews Endocrinology*, 18(9):525–539, 2022.

Vivian A Fonseca. Defining and characterizing the progression of type 2 diabetes. *Diabetes care*, 32(Suppl 2):S151, 2009.

Marc Gregory Yu, Daniel Gordin, Jialin Fu, Kyoungmin Park, Qian Li, and George Liang King. Protective factors and the pathogenesis of complications in diabetes. *Endocrine reviews*, 45(2): 227–252, 2024.

Mikhail S Dzeshka, Gregory YH Lip, Viktor Snezhitskiy, and Eduard Shantsila. Cardiac fibrosis in patients with atrial fibrillation: mechanisms and clinical implications. *Journal of the American College of Cardiology*, 66(8):943–959, 2015.

Robert O Bonow, Douglas L Mann, Douglas P Zipes, and Peter Libby. *Braunwald's heart disease e-book: A textbook of cardiovascular medicine*. Elsevier Health Sciences, 2011.

APPENDIX

A MATHEMATICAL NOTATIONS

The main mathematical notations of this paper is shown in Table 3.

Table 3: Main mathematical notations.

Notation	Description
$\mathbf{x}_u(t_k)$	Risk factors vector of patient u at time t_k
$\mathbf{y}_u(t_k)$	Marker status vector of patient u at time t_k
$\mathcal{V}$	Set of markers (nodes)
p_j	The j-th trajectory: $< v_1^j, v_2^j, ..., v_{\lvert p_j \rvert}^j >$
n	Number of predefined markers (nodes)
m	Number of predefined trajectories (hyperedges)
v_i^j	The i-th marker in trajectory p_j
$\mathcal{H}$	Disease progression hypergraph: $(\mathcal{V}, \mathcal{E})$
p_j^u	Patient u's temporally detailed trajectory along p_j
$\mathcal{H}^u$	TD-Hypergraph of patient u: $(\mathcal{V}, \mathcal{E}^u)$
e_j^u	TD-Hyperedge of u along p_j

B TRAINING ALGORITHM

After integrating the ODE from the latest observed timestamp t_k to t_{k+1}, we obtain $\mathbf{S}(t_{k+1}) \in \mathbb{R}^{n \times d}$, the hidden representations of all n markers at time t_{k+1}. These embeddings are then mapped to prediction scores for each marker, followed by a sigmoid activation to estimate the probability of presence for each marker at t_{k+1}. The model is trained by minimizing the binary cross-entropy (BCE) loss between the predicted probabilities and the ground-truth marker statuses.

The overall training process is detailed in **Algorithm 1** below. In particular, we adopt an auto-regressive training loop: for each patient, the model integrates the continuous dynamics forward in time, using the hidden state at t_k to predict marker outcomes at t_{k+1}. At each step, the TD-Hypergraph Laplacian computed at time t_k guides the flow of information, capturing fine-grained trajectory dynamics and marker dependencies.

Algorithm 1 Training procedure of TD-HNODE

```
Require: • Encounter sequences for $N$ patients:
           $\{\mathbf{x}_u(t_1), \dots, \mathbf{x}_u(t_{l_u});\ \mathbf{y}_u(t_1), \dots, \mathbf{y}_u(t_{l_u})\}_{u=1}^{N};$
         • TD-Hypergraphs: $\{\mathcal{H}^u\}_{u=1}^{N}$
Ensure: Model parameters $\mathbf{\Theta'}$
Initialize all parameters $\mathbf{\Theta'}$
for epoch in 1 : MaxEpoch do
    for each patient $u$ do
        Initialize hidden state $\mathbf{S}_u(t_1)$
        for timestamp $t_k \leftarrow t_1 : t_{l_u}$ do
            Compute incidence matrix $\mathbf{H}_p(t_k)$ (Eq. 7)
            Compute hyperedge weights $\mathbf{W}_p(t_k)$ (Eq. 9)
            Compute TD-Hypergraph Laplacian $\tilde{\mathbf{L}}(t_k)$ (Eq. 10)
            Update state: $\mathbf{S}_u(t_{k+1}) \leftarrow$ ODESolver($\mathbf{S}_u(t_k), \mathbf{x}_u(t_k), \tilde{\mathbf{L}}(t_k), [t_k, t_{k+1}]$)
            $\hat{\mathbf{y}}_u(t_{k+1}) =$ Sigmoid($\mathbf{S}_u(t_{k+1})$)
            Compute loss $\mathcal{L} \leftarrow$ BCE($\hat{\mathbf{y}}_u(t_{k+1}), \mathbf{y}_u(t_{k+1})$)
        end for
    end for
    Update $\mathbf{\Theta'}$ via gradient descent on accumulated loss
end for
return $\mathbf{\Theta'}$
```

C COMPUTATIONAL COMPLEXITY

Assume the average number of timestamps per patient sequence is $\hat{L}$, the batch size is B, the number of markers (nodes) is n, the number of hyperedges is m, the number of attention heads is $\hat{h}$, and the hidden dimension is $\hat{d}$. We denote the average number of markers per hyperedge as n_e and the number of Runge-Kutta steps in Neural ODE as s.

- Attention-based incidence matrix (Eq. 6): The query matrix dimensions are $Q \in \mathbb{R}^{B\times\hat{h}\times m\times\hat{d}}$ and the key matrix dimensions are $K \in \mathbb{R}^{B\times\hat{h}\times m\times n_e\times\hat{d}}$. The dot-product attention computation has complexity $O(B \cdot \hat{h} \cdot m \cdot n_e \cdot \hat{d})$ per timestamp.
- Hyperedge weight matrix (Eq. 9): Self-attention pooling within each hyperedge costs $B \cdot m \cdot n_e^2 \cdot \hat{d}$, and computing the pairwise trajectory correlation matrix $W_p \in \mathbb{R}^{m\times m}$ costs $B \cdot m^2 \cdot \hat{d}$. Total complexity is $O(B \cdot (m \cdot n_e^2 + m^2) \cdot \hat{d})$.
- TD-Hypergraph Laplacian (Eq. 10): Matrix multiplications for constructing $\tilde{L}$ require $O(B \cdot n \cdot m)$ operations per timestamp.
- ODE solver: Each message passing operation during one Runge-Kutta step costs $O(B \cdot n \cdot m \cdot \hat{d})$, and since the solver performs s such steps for numerical integration, the total cost is $O(B \cdot s \cdot n \cdot m \cdot \hat{d})$ per timestamp.

The overall per-batch complexity of TD-HNODE is

$$T_{\text{total}} = O(B \cdot \hat{L} \cdot (\hat{h}mn_e\hat{d} + mn_e^2\hat{d} + m^2\hat{d} + nm + snm\hat{d})),$$

and since $n_e \leq n$, we can further bound it by

$$T_{\text{total}} \leq O\big(B \cdot \hat{L} \cdot \hat{d}(mn^2 + m^2 + snm)\big).$$

Given our settings with $n \in [20, 30]$, $m \in [10, 15]$, and $\hat{L} \leq 20$, the dominant cost is the ODE solver $O(B \cdot \hat{L} \cdot s \cdot n \cdot m \cdot \hat{d})$, and overall complexity scales linearly with sequence length and the number of hyperedges.

D EXPERIMENTS

D.1 RISK FACTORS

The risk factors were defined below by our clinical co-author (MD) based on established expertise and supported by the literature on diabetes complications (Tomic et al., 2022).

Table 4: List of 34 risk factors used in the study.

SEX_CD	GFR
HDL	Triglycerides
Beta_blockers	CCB
DPP4i	Lipid
Loop	Metformin
Non_loop	RAS
Sulfonylurea	Thiazolidinedione
Alcohol_use_disorder	Angina_flag
Cardiovascular_Disease	Chronic_kidney_disease
Drug_use_disorder	End_Stage_Renal_Disease
Exercise	Gestational_diabetes
History_of_Myocardial_Infarction	History_of_stroke
HIV_AIDS	Hypercholesterolaemia
Lower_extremity_amputation	Myocardial_Infarction_MI
Organ_transplant	Peripheral_vascular_disease
Photocoagulation	Pregnancy
Retinopathy_intravitreal_injections	Secondary_diabetes

D.2 COMPLICATION MARKERS

The 21 diabetes complication outcome markers were defined below by our clinical co-author (MD) based on established clinical expertise and supported by the literature on diabetes complications (Tomic et al., 2022). In our formulation, we treat all 21 markers as **irreversible**. Although some markers such as ‘HbA1c Low’, ‘HbA1c High’, ‘Poor Lipid’, and ‘Poor BP’ are laboratory test results that may fluctuate over time, we emphasize their *first occurrence* as an indication that the patient has progressed to this stage of disease or has experienced this level of abnormality. Following clinical guidance, we therefore model the initial onset of each marker as a significant progression event that remains active in the disease trajectory representation.

Table 5: List of 21 diabetes complication markers and their abbreviations used in Figure 4.

HbA1c Low	HbA1c High	Hypoglycemia (Hypo)
Obesity	Nephropathy (Neph)	Neuropathy (Neuro)
Foot Ulcer (Ulcer)	Cancer	Hypertension (HTN)
Poor Lipid	Poor BP	Retinopathy (Reti)
Depression (Depress)	DKA (Keto)	Visual Impairment (VI)
Blindness and Vision Loss (Vision)	Cerebrovascular Disease (CVD)	Stroke
Atrial Fibrillation (AFib)	Cardiac Revascularization (Cardiac)	Heart Failure (CHF)

D.3 DISEASE PROGRESSION PATHWAYS

The predefined hyperedges (progression pathways) were determined below with guidance from our clinical co-author (MD) and supported by established medical literature (Fonseca, 2009; Yu et al., 2024).

- HbA1c High → Poor Lipid → Hypertension / Poor BP → Atrial Fibrillation → Heart Failure
- HbA1c High → Obesity
- HbA1c High → Retinopathy → Visual Impairment → Blindness and Vision Loss
- HbA1c Low → Hypoglycemia
- HbA1c High → DKA
- HbA1c High → Poor Lipid → Hypertension / Poor BP → Cardiac Revascularization
- HbA1c High → Depression
- HbA1c High → Poor Lipid → Hypertension / Poor BP → Cerebrovascular Disease → Stroke
- HbA1c High → Neuropathy → Foot Ulcer
- HbA1c High → Nephropathy

D.4 DATASET DETAILS

We provide additional details about the two datasets used in our study.

University Hospital Dataset. This study was approved by the Institutional Review Board (IRB) of our institution. This dataset contains longitudinal EHR sequences for 2,415 diabetic patients collected from a regional medical network affiliated with our institution. Each patient record consists of a time-ordered sequence of hospital encounters, including structured clinical information such as laboratory test results, vital signs, medications, and diagnosis codes.

MIMIC-IV Dataset. MIMIC-IV (Johnson et al., 2023) is a publicly available EHR dataset collected from the Beth Israel Deaconess Medical Center. Although not specifically designed for diabetes, we identified 902 patients with at least one diabetes-related complication by mapping ICD-9/10 diagnosis codes to our predefined marker set $\mathcal{V}$.

Preprocessing. For both datasets, we organized each patient's data as a sequence of 20 encounters, with each encounter containing a risk factor vector $\mathbf{x}_u(t_k)$ and a binary complication marker vector $\mathbf{y}_u(t_k)$. For the University Hospital dataset, the raw encounter sequence lengths ranged from 10 to 40. To standardize the input format, we fixed the sequence length at 20. The basic statistics of both datasets are shown in Table 6. For patients with fewer than 20 encounters, we applied padding at the end of the sequence; for those with more than 20, we selected the latest 20 encounters, as disease progression events tend to occur in later stages of follow-up.

Table 6: Dataset statistics for University Hospital and MIMIC-IV.

Dataset	Number of Encounters			Time Span (Months)		
	Min	Avg	Max	Min	Avg	Max
University Hospital	10	15	40	19.4	68.6	121.7
MIMIC-IV	20	20	20	6.4	73.1	177.1

Missing values in the risk factor vectors were imputed using the most recent non-missing value from prior encounters (i.e., last-observation carried forward). This approach preserves temporal consistency and aligns with clinical practice, where outdated test results are often referenced until updated.

In addition, under guidance from clinical collaborators, several continuous-valued physiological indicators were discretized into clinically meaningful categories. Specifically:

- **GFR** values were discretized into `GFR_NORM` ($\geq$ 90), `GFR_Decrease_Slight` ($60 \leq$ GFR < 90), and `GFR_Decrease_Severe` (< 60).
- **HDL** values were mapped to `HDL_Good` ($\geq$ 60), `HDL_Normal` ($40 \leq$ HDL < 60), and `HDL_Bad` (< 40).
- **Triglycerides** were categorized into `Triglycerides_Good` ($<$ 150), `Triglycerides_LowRisk` ($150 \leq$ TG $<$ 199), and `Triglycerides_HighRisk` ($\geq$ 199).

These discrete categories were embedded as input tokens for our model.

For the MIMIC-IV dataset, only structured diagnosis codes were used to construct the complication marker vectors $\mathbf{y}_u(t_k)$ by mapping ICD-9/10 codes to the predefined marker set $\mathcal{V}$. Risk factor inputs were not utilized due to sparsity and inconsistency across patient records.

Hypergraph Construction. We constructed a disease progression hypergraph $\mathcal{H}$ based on expert-validated trajectories of diabetes complications. Each trajectory forms a hyperedge capturing high-order progression patterns among markers, serving as the structural backbone for constructing patient-specific TD-Hypergraphs in our framework.

D.5 IMPLEMENTATION DETAILS

We applied the same label preprocessing strategy to both datasets: **for each complication marker, only its first occurrence (onsite) was used**. This transformed the problem from simple state classification to the actual challenge, i.e., **disease onset prediction** — whether a new complication would occur in the next encounter. For both datasets, we randomly split patients into training, validation, and test sets using an 8:1:1 ratio.

We implemented all models using PyTorch and conducted training on a cluster of 8×NVIDIA A100 GPUs (80GB). Our TD-HNODE model was trained using the Adam optimizer with a learning rate of 1e-4, weight decay of 1e-6, and a batch size of 1. Training was run for up to 200 epochs, with early stopping applied based on the validation loss (patience = 5).

We used 128-dimensional embeddings for both discrete token inputs and continuous time position embedding. The hyperedge attention encoder consisted of 2 attention layers with 8 attention heads each, a feed-forward expansion factor of 4, GELU activation, and dropout rate of 0.1. Positional encodings were learnable, and token embeddings were initialized using a uniform distribution.

The Neural ODE module modeled continuous-time latent dynamics over the TD-Hypergraph using a fixed-step Runge-Kutta 4th-order method (RK4) with 10 solver steps. The input to the ODE consisted of the hypergraph-enhanced representations obtained from the TD-Hypergraph Laplacian, and its outputs were decoded into complication marker probabilities via a sigmoid layer.

Source code has been included in the Supplementary Material for reproducibility.

D.6 BASELINES DETAILS

To evaluate the effectiveness of TD-HNODE, we compare it against representative baselines from several major categories:

(1) Sequential Models:

- **T-LSTM** Baytas et al. (2017): A time-aware LSTM variant designed to handle irregularly sampled patient records.
- **ContiFormer** Chen et al. (2024b): Extends the Transformer architecture by redefining self-attention to operate over time-evolving latent trajectories.

(2) Temporal Graph Neural Networks:

- **MegaCRN** Jiang et al. (2023): A discrete-time GNN model that combines graph convolution with gated recurrent units (GRU), operating on temporal graphs represented as discrete-time snapshots.
- **TGNE** Cheng et al. (2024): A continuous-time GNN that constructs event-based structural messages to model evolving temporal graphs in a fine-grained manner.

(3) Temporal Hypergraph Neural Networks:

- **DHSL** Wang et al. (2024a): Combines a hypergraph convolution network with a GRU to jointly model high-order spatial correlations and temporal dependencies.
- **HyperTime** Younis and Ahmadi (2024): Constructs dynamic hypergraphs from time series segments and applies LSTM-enhanced hyperedge convolutions to model evolving temporal patterns.

(4) Neural ODE-based Models:

- **NODE** Chen et al. (2018): A foundational continuous-time model that captures smooth temporal dynamics via ODE-based latent evolution.
- **CODE-RNN** Coelho et al. (2025): Combines Neural ODEs with recurrent networks to model temporal dynamics in time-series data.

As for DHSL and HyperTime, both adopt a discrete-time hypergraph neural network: They divide continuous time domain into discrete time intervals (different snapshots). Within each time interval, they construct a static hypergraph snapshot and use hypergraph convolution to extract spatial structure. Then, a recurrent module (GRU/LSTM) is applied across the snapshots to propagate features over time. This design may encounter difficulties in modeling the subtle temporal progression patterns on irregular time data (as in our case).

To ensure fairness, we customized each method to our task setting. Specifically, for models without structual inputs, *i.e.,* Categories (1) and (4), we concatenate risk factors vector $\mathbf{x}$ and marker status vector $\mathbf{y}$ as inputs. For graph-based models, *i.e.,* Categories (2), we break the TD-Hypergraph $\mathcal{H}$ into standard graph with pariwise edge. For models that assume discrete time, *i.e.,* MegaCRN, DHSL, HyperTime, we segment the temporal graph or hypergraph into fixed-length snapshots by treating each patient encounter as a separate timestamp. That is, we construct a static graph (or hypergraph) for each encounter and stack them sequentially as discrete time steps. For graph-based that assume continous time, *i.e.,* TGNE, we treat each encounter as an individual event, ordered by its timestamp. We convert the temporally detailed hypergraph into a sequence of timestamped edges.

D.7 ADDITIONAL EXPERIMENTS ON CHRONIC DISEASE

To further evaluate the generalizability of our framework, we incorporated an **additional chronic disease (cardiovascular disease)** using the publicly available MIMIC-IV dataset Johnson et al. (2023). ICD-9/10 codes were mapped to five clinically recognized markers: Hypertension, Atrial Fibrillation, Heart Failure, Cerebrovascular Disease / Stroke, and Myocardial Infarction. Based on prior clinical studies Dzeshka et al. (2015); Bonow et al. (2011), we defined three representative progression pathways:

- Hypertension → Atrial Fibrillation → Heart Failure
- Hypertension → Myocardial Infarction → Heart Failure
- Hypertension → Cerebrovascular Disease / Stroke

This preprocessing resulted in 1,665 patients (train/validation/test = 1,332/166/167), with dataset statistics summarized in Table 7.

Table 7: Statistics of the cardiovascular disease dataset.

Dataset	Number of Encounters			Time Span (Months)		
	Min	Avg	Max	Min	Avg	Max
Cardiovascular Disease	9	14	20	4.2	53.3	94.2

We compared TD-HNODE with all baseline methods, and the results are presented in Table 8.

Table 8: Performance comparison on the cardiovascular disease dataset.

Model	Accuracy	Precision	Recall	F1-score
T-LSTM	0.701	0.126	0.613	0.179
ContiFormer	0.796	0.189	0.765	0.266
MegaCRN	0.744	0.167	0.759	0.233
TGNE	0.761	0.175	0.801	0.247
DHSL	0.740	0.150	0.717	0.232
HyperTime	0.752	0.160	0.734	0.231
NODE	0.786	0.152	0.689	0.227
CODE-RNN	0.779	0.166	0.699	0.190
TD-HNODE	**0.804**	**0.193**	**0.818**	**0.291**

As shown in Table 8, TD-HNODE consistently outperforms all baselines on the cardiovascular disease dataset, particularly in recall and F1-score. These findings demonstrate that our framework effectively captures the progression of chronic diseases beyond diabetes and highlight its potential for generalization when expert-defined progression pathways are available.